

Theoretical prediction of a transient accumulation of nanoparticles at a well-defined distance from an electrified liquid-solid interface

Crystal Chan, Enno Kätelhön, and Richard G. Compton*

Department of Chemistry, Physical and Theoretical Chemistry Laboratory, Oxford University,
South Parks Road, Oxford, OX1 3QZ, United Kingdom.

Abstract

The Brownian motion of nanoparticles near liquid-solid interfaces is at the heart of evolving technologies: Recent developments in the sensing of nano-objects and energy storages based on electro-active colloidal solutions crucially rely on the understanding and, even more, on the control of particle transport near charged surfaces.

On the basis of the Nernst-Planck equation, the Gouy-Chapman model, and an established model of near-wall hindered diffusion, this work predicts transient and *highly-localised* accumulations of nanoparticles at a *well-defined* distance from an electrified surface following a potential being applied. The interplay of electrostatics and near-wall hindered diffusion yields entirely unexpected effects: Nanoobjects temporarily accumulate near the interface while even small electric potentials applied at the surface can dramatically enhance the mass transport of nano-objects towards it.

1 Introduction

Recent years saw a growing interest in the electrochemistry of individual nanoparticles. This, on the one hand, has been stimulated by the newly-available nano-impact technique^{1–5} which enables the detection and characterisation of individual nanoparticles⁶. An electrode is herein set in contact with an analyte solution and biased versus the solution potential. Analyte nanoparticles may then stochastically reach the electrode by virtue of their Brownian motion and react due to their intrinsic electrochemical

*Corresponding author: Richard G. Compton, richard.compton@chem.ox.ac.uk

properties while their reaction is monitored in the electrode current. The technique has been shown to be highly versatile beyond the detection of metallic nanoparticles and applications in the sensing of viruses⁷, bacteria⁸, enzymes^{9;10}, and red blood cells¹¹ have been discussed. On the other hand, there is a significant interest in using colloidal (nano-)particle solutions as new materials for energy storage where notable applications include semi-solid flow batteries^{12–14} and flow capacitors¹⁵.

Understanding mass transport at charged surfaces is essential to all the above research which is centred around the charge transfer between a nanoparticulate analyte and an electrode. The diffusive mass transport of nanoparticles near an interface is however complicated compared to that of a small molecule: Due to the viscosity of water in conjunction with its slippage properties at the interface, the diffusion coefficient of nano-objects varies with the distance from the surface. Diffusion hence cannot be described by diffusion equation in its simplified form:

$$\frac{\partial c(x, t)}{\partial t} = D \Delta c(x, t) \quad (1)$$

but requires the solution of the more general equation:

$$\frac{\partial c(x, t)}{\partial t} = \nabla \cdot (D(x) \nabla c(x, t)) \quad (2)$$

where c is the analyte concentration at the position x and the time t , D is the diffusion coefficient, and Δ is the Laplace operator $\Delta = \nabla \cdot \nabla$. The implications of this altered diffusion on electrochemical measurements at *high* electrolyte concentrations have been extensively discussed in previous literature^{16–18}.

In addition to near-wall hindered diffusion, electrostatics may play an important role in the above applications where electrochemical reactions of nanoparticles typically occur in the presence of an electrolyte. This electrolyte ensures the conductivity of the solution, screens the electric field in the bulk, and establishes a potential drop confined to the proximity to the interface as characterised by the Debye length. Electrochemical reactions may take place if an analyte is located within the tunnelling distance of a few Ångström from the electrode and the potential drop is sufficiently large to drive the reaction. In the case of a Debye length exceeding the tunnelling distance, the diffusive mass transport of a charged analyte is altered by the influence of the electric field induced by the potential drop and must be considered. While nanoscale mass transport of a small molecule in the absence of an electric field can be described by diffusion equation, the interfacial mass transport at low electrolyte concentrations requires the solution of Nernst-Planck equation of the form:

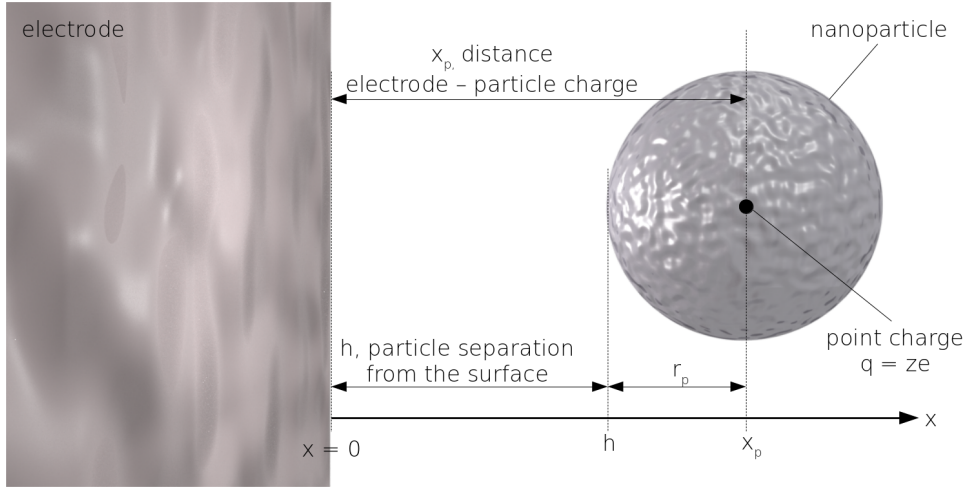


Figure 1: Illustration of the geometry considered. The mass transport of nanoparticles is modelled in one dimension perpendicular to the electrode surface. Particles further feature a radius r_p and carry the charge $q = ze$ which is located centrally inside the particle.

$$\frac{\partial c(x,t)}{\partial t} = \nabla \cdot \left(D(x) \nabla c(x,t) + \frac{zF}{RT} D(x) c(x,t) \nabla \phi(x) \right) \quad (3)$$

for a given potential distribution $\phi(x)$ and an analyte that carries the charge ze and does not perturb the equilibrium distribution of the electrolyte. If the electrolyte has to be modelled explicitly, the full Nernst-Planck-Poisson equation has to be solved. The latter case is typically referred to as "weakly supported voltammetry" and has previously been discussed in much detail.^{19–23}

This work investigates the interplay of electrostatics *and* near-wall hindered diffusion on the basis of the Nernst-Planck equation, the Gouy-Chapman model, and a well-validated model of near-wall hindered diffusion. First, we predict that this interplay leads to a large up-concentration of analyte around a well-defined distance from the electrode. This prediction is entirely unexpected and counter-intuitive. Second, our results demonstrate that reduced electrolyte concentrations can dramatically enhance the mass transport of analyte towards the electrode even at low over- or under-potentials.

2 Theoretical Model

We consider the one-dimensional Cartesian geometry of a macro-electrode set in contact with an analyte solution. The solutions comprises a low concentration of electro-active nanoparticles as well as a low concentration of an inert electrolyte solution and is hence 'weakly supported'. An illustration of the geometry can be found in Figure 1.

The particle mass transport is assumed to be solely due to diffusion and migration in an external

electric field, and can hence be described by the Nernst-Planck equation (3), which in the context of this work is written in the form:

$$\begin{aligned} j &= -D(x)\nabla c(x,t) - \frac{zF}{RT}D(x)c(x,t)\nabla\phi(x) \\ \frac{\partial c(x,t)}{\partial t} &= -\nabla \cdot j - P(x,t) \end{aligned} \quad (4)$$

where $c(x,t)$ is the concentration* of particles. $D(x)$ is the position-dependent particle diffusion coefficient and $P(x,t)$ is an additional term which represents the Faradaic interaction of the particles with the electrode, and are both addressed below. The equation is further solved subject to no-flux boundary conditions at the electrode and in the bulk:

$$\begin{aligned} j(x=r_p) &= -D(x)\nabla c(r_p,t) - \frac{zF}{RT}D(x)c(r_p,t)\nabla\phi(r_p) = 0 \\ j(x=x_{max}) &= -D(x)\nabla c(x_{max},t) - \frac{zF}{RT}D(x)c(x_{max},t)\nabla\phi(x_{max}) = 0 \end{aligned} \quad (5)$$

where x_{max} is set in sufficient²⁵ distance from the electrode to ensure that the choice of the upper boundary condition does not effect processes at the interface:

$$x_{max} = 6\sqrt{D_{\infty} t_{max}} + r_p \quad (6)$$

where t_{max} is duration of the simulated experiment. The initial distribution of particles in solution is further assumed to be uniform[†]:

$$c(x,t=0) = \begin{cases} c^* & \text{for } r_p < x < x_{max} \\ 0 & \text{everywhere else} \end{cases} \quad (7)$$

The Brownian motion of the particles at the interface is altered with respect to the bulk. The presence

*We note that depending on the size of the electrode surface, at the low particle concentrations considered in this work, the flux of particles towards or away from the electrode is stochastic rather than continuous. In such a context the one-dimensional particle concentration can be equally interpreted as a probability density of finding particle in a specific distance from the electrode.²⁴

[†]For clarity we note that, at the microscale, the distribution of nanoparticles at the beginning of the experiment, i.e. for $t < 0$, cannot be uniform which is due to the discrete nature of the particles. The particle positions, in absence of both an electric field and an adsorbing electrode, are however affected by thermal fluctuations. In the case of diffusion these fluctuations manifest in a non-uniform concentration at the micro scale and concentrations must be interpreted as probability densities. If however evaluated at the macro scale, for instance at a macroelectrode exposed to a nanoparticle solution for the here-investigated time scales, the concentration may be approximated as a one-dimensional concentration profile $c(x)$. In this latter case, we integrate the actual concentration $c(x,y,z)$ with respect to y and z to determine $c(x)$ which, following the law of large numbers, converges to a uniform concentration $c(x) = \text{const}$. It is herein important to note that $c(x) = \text{const}$. satisfies Eqn (2) and (3) for $dc/dt = 0$ and in absence of an electric field even if near-wall hindered diffusion is included in the model and is hence a valid assumption for the initial state of the system at $t < 0$.

of the interface in conjunction with the viscosity of the solvent and its slippage characteristics at liquid-solid boundaries give rise to a drop in the diffusion coefficient. While in sufficient distance, the diffusion coefficient asymptotically reaches the bulk diffusion coefficient, it falls to zero at the interface. The effect can be approximated through an equation established²⁶ by Bevan and Prieve:

$$\begin{aligned} D(x) &= \frac{6h^2 + 2r_p h}{6h^2 + 9r_p h + 2r_p^2} D_\infty \\ &= \frac{6(x - r_p)^2 + 2r_p(x - r_p)}{6(x - r_p)^2 + 9r_p(x - r_p) + 2r_p^2} D_\infty \end{aligned} \quad (8)$$

where $h = x - r_p$ denotes the elevation of the particle from the surface, i.e. the distance between the edge of the particle and the electrode as illustrated in Figure 1. D_∞ is the bulk coefficient which is calculated via the Stokes-Einstein equation:

$$D_\infty = \frac{k_B T}{6\pi\eta r_p} \quad (9)$$

The mass transport of the nanoparticles is affected by the electric field that arises from the potential applied at the electrode and positions of ions in solution.

$$\epsilon_0 \epsilon_r \Delta \phi(x) = - \sum_i x_i q_i \quad \text{with} \quad \phi(0) = \phi_e \quad \text{and} \quad \phi(x \rightarrow \infty) = 0 \quad (10)$$

where the contribution of the ions is considered in the sum in the Poisson equation and the potential of the electrode is considered through the boundary condition at $x = 0$. x_i and q_i are the positions and charges of the individual ions, respectively, and ϕ_e is the electrode potential. We further consider a monovalent and fully dissolved electrolyte, i.e. $|z_i| = 1$ and the molar amounts of ions in solution equal the amount of electrolyte added. In addition, various assumptions are made. First, ions do not feature a volume which is a good approximation at low ion concentrations and moderate electrode polarizations.²⁷ Second, the distribution of ions is at equilibrium at any time, which is justified by the fact that the ion diffusion coefficient is much greater than the diffusion coefficient of the considered particles. Third, the charge and the volume of the particles is sufficiently small to not perturb the equilibrium distribution of ions at the interface. And fourth, the particle concentration is sufficiently dilute to ensure that there is no interaction between particles. The assumptions made resemble the Gouy-Chapman model of the electrode-electrolyte interface, which results in the following equilibrium potential:

$$\frac{\tanh(\frac{\Theta}{4})}{\tanh(\frac{\Theta_0}{4})} = e^{-\frac{x}{\kappa^{-1}}} \quad \text{with} \quad \Theta = \frac{F}{RT}(E - E_f^0) \quad (11)$$

where E_f^0 is the formal potential and κ^{-1} is the Debye length:

$$\kappa^{-1} = \frac{1}{F} \sqrt{\frac{\epsilon_0 \epsilon_r RT}{2F^2 c^*}} \quad (12)$$

Our simulation models a reaction in which the particle instantaneously and entirely electro-dissolves in the proximity of the electrode which is in excellent agreement²⁸ with experimental observations. To this end, we include a tunnelling term^{29;30} $P(x, t)$ in the Nernst-Planck equation which accounts for the stochastic annihilation of particles where the reaction probability varies with the particles distance from the electrode:

$$P(x, t) = c(x, t) \nu e^{-\beta h} \quad (13)$$

where β is solvent-dependent parameter featuring a value³¹ of about 1.59 \AA^{-1} in water. ν is a parameter featuring the unit of frequency and represents the rate at which the tunnelling probability $e^{-\beta x}$ is evaluated. We determine ν by comparison with Cottrell equation for the case that the particle carries a charge of zero and is not affected by near-wall hindered diffusion.

The rate $j_e(t)$ of particles reacting at the electrode is calculated from the change in mass of all particles in the system. To this end, we integrate the concentration over all space and determine how this value changes with time:

$$j_e(t) = -\frac{d}{dt} \int_{r_p}^{x_{max}} dx c(x, t) \quad (14)$$

We note that the lower integration boundary is set to the particle radius r_p as x is defined as position of the particle centre.

As illustrated in the above theoretical model, our findings are based on well-established physical concepts, namely the Nernst-Planck equation, the Gouy-Chapman model, and a established model of near-wall hindered diffusion, which set a strong physical basis for this work.

3 Computational Methods

Custom software was developed for the purpose of this study and is used for all calculations. Herein partial differential equations are discretised in time and space, and solved via the finite differences method. Software is written in *C++* and data is processed and visualised in *Python* via the *NumPy* and *matplotlib* packages.

4 Results and Discussion

This section presents numerical solutions to the above theoretical model of destructive nano-impact experiments under the influence of hindered diffusion and electrostatics. Initially, the electrode is not potentiostated and electrolyte ions as well as analyte nanoparticles distribute uniformly across the solution. Then, a potential is applied at the electrode and the electrolyte ions effectively instantaneously rearrange in response to it, forming a time-invariant potential distribution. It is assumed that this potential gradient is solely due to charges on the electrode and the spatial distribution of electrolyte ions, and any charge on nanoparticles does not measurably perturb the potential gradient. As the electrolyte ions are much smaller than nanoparticles and thus diffuse and migrate faster than nanoparticles, the solution potential can in good approximation be assumed to equilibrate instantaneously compared to the time scale of a nano-impact and a constant potential gradient is assumed at time zero. Nanoparticles then undergo destructive nano-impacts and, in the here established model, react instantaneously upon impacting on the electrode which is in line with experimental observations where the reaction is often faster than the bandwidth of the potentiostat (see Section). The resulting rate of particles reacting, i.e. the particle flux ($\text{particles s}^{-1} \text{m}^{-2}$), to the electrode is calculated as a function of time from $t = 0 \text{ s}$ and the temporal evolution of the corresponding nanoparticle concentration profiles is calculated.

The initial bulk concentration of nanoparticles, c^* , is chosen to be $1 \times 10^{-12} \text{ M}$ in all simulations, which is a typical value used in nano-impact experiments¹. It is though noted that particle fluxes are proportional to c^* and simulation results can hence be easily transformed to describe other scenarios.

The complexity of the investigated physical system arises at least in part from its intricate dependency on a large number of parameters. In the context of this work we have therefore put significant effort into a dimensional analysis which however allows only few simplifications. The total number of relevant parameters cannot be less than four which we chose to be the particle charge, the electrode potential, the particle radius, and the Debye length. All results are hence functions of these four independent parameters and, due to the sheer quantity of relevant data, cannot be presented exhaustively in a single

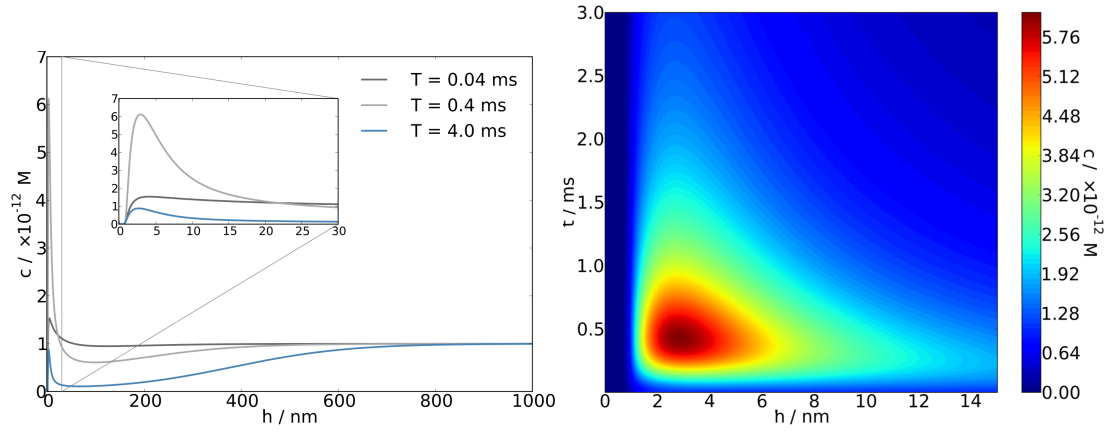


Figure 2: Concentration profiles a) plotted at different times and b) illustrated as a contour plot. The nanoparticle charge is -50, the electrode potential is 100 mV, the Debye length of the solution is set to 100 nm, which corresponds to $9.42 \mu\text{M}$ of 1:1 monovalent supporting electrolyte, and the nanoparticle radius is 100 nm.

article. We instead pick few practical examples and separately investigate the impact of each parameter on the system for a qualitative explanation. Various parameters are addressed separately in the following: First, the effect of the nanoparticle charge is investigated, followed, second, by the electrode potential, third, the nanoparticle radius, before, lastly, we examine the influence of the Debye length on the particle flux.

4.1 Nanoparticle Charge

Almost all individual nanoparticles in solution are charged. As particles feature large surface-to-volume ratios, van-der-Waals forces in neutral particle systems are significant and lead to agglomeration and aggregation unless the systems thermal energy is sufficient, which is not the case in most experimental conditions. Hence, surface charges are often induced deliberately in the nanoparticle synthesis to stabilise the particle population. This can for instance be achieved through the addition of capping agents with charged groups, such as citrate, which are commonly used in particle populations investigated via nano-impacts. Understanding the effect of the nanoparticle charge is hence crucial.

We first consider the exemplary case of a nanoparticle featuring a charge of 50 and a radius of 100 nm. The electrode potential is set to 100 mV and the Debye length is 100 nm which corresponds to $9.42 \mu\text{M}$ of a 1:1 monovalent supporting electrolyte. The calculated temporal evolution of the particle concentration is shown in Figure 2.

Figure 2 a) reveals an exciting and unexpected result: We observe an elevated concentration of nanoparticles near the electrode surface at $t = 0.04 \text{ ms}$ and $t = 0.4 \text{ ms}$ which is localised in a well-defined

distance from the surface. The amount of accumulated particles grows to a maximum value of more than six times the initial concentration, before the peak gradually decreases with time. 2 b) additionally shows the same simulation as a contour map in time and space.

The accumulation of nanoparticles near the electrode surface is a new physical insight, which, as we will see below, provides an easy and fast way to concentrate nanoparticles near interfaces in a broad range of sensing scenarios.

The occurrence of the accumulation is caused by an interplay of hindered diffusion and electrostatics: Charged particles move towards the electrode by the virtue of both diffusion, i.e. particles are consumed at the electrode and a concentration gradient is established, and migration within the potential gradient. However, since the diffusion coefficient, $D(x)$, drops with the particle distance from the electrode, the mass transport due to diffusion,

$$j_d(x, t) = -D(x) \frac{\partial c(x, t)}{\partial x} \quad (15)$$

and migration,

$$j_m(x, t) = -\frac{zF}{RT} D(x) c(x, t) \frac{\partial \phi(x)}{\partial x} \quad (16)$$

both slow down near the interface. As a result, nanoparticles accumulate near the electrode as they continuously reach this region by migration while the mass transport away from this region to the electrode surface is hindered. As the reaction proceeds, the particle accumulation reaches a maximum. At this time, the diffusive flux away from the accumulation region to the bulk that is due to the concentration gradient built up is countered by migration, $j_D \approx j_m$ for $x > x_{peak}$. Simultaneously, the rate of mass transport from the accumulation region to the electrode is enhanced due to the increased concentration gradient and the elevated concentration in its proximity. The electrode continues to slowly consume material from the accumulation region while the bulk is depleted to a point where the electric field does not reach out far enough to attract nanoparticles from the bulk further away. As a result, the peak in the concentration of nanoparticles disappears gradually with time.

We next extend the investigation to nanoparticles with other values of charge and study the rate j_e at which particles are consumed at the electrode. The corresponding fluxes of nanoparticles with the charges -50, -1, 0, 1 and 50 are shown in Figure 3 where we plot the flux of reacting particles per electrode area from the moment on at which the electrode is potentiostated.

As we can see from the figure, when the nanoparticle charge is 50, the flux is the smallest among the

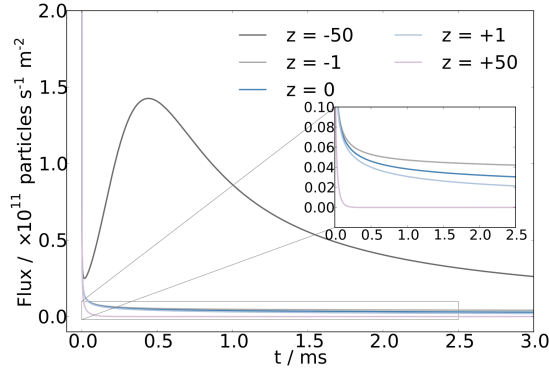


Figure 3: Comparison of calculated fluxes of nanoparticles featuring different charges. All other parameters equal those used in Figure 2.

nanoparticles studied as particles experience the strongest repulsion from the positively charged electrode and hence migrate away from the interface. Conversely, for nanoparticles with charge -50, the flux is the largest as these particles experience the strongest attraction from the positively charged electrode.

Moreover, when the nanoparticle charge is -50, there is a peak in the flux at around 0.4 ms which one may not intuitively anticipate. This observation can be understood via the temporal evolution of the particle concentration, shown in Figure 2. The mass transport as described by the Nernst-Planck equation features a diffusion term and a migration term, which are proportional to the concentration gradient and the concentration, respectively. As the concentration of particles near the interface peaks while the reaction proceeds, a peak in the flux is observed due to the elevated concentration gradient and absolute concentration near the interface. Such peak is not observed in nanoparticles with charges other than -50, as the rates of migration are not fast enough for the formation of an accumulation region.

In summary, when the nanoparticles and the electrode are oppositely and appropriately charged, an unexpected yet large concentration of nanoparticles at a well-defined distance from the electrode and a peak in the particle flux are observed. We further demonstrate that the mass transport is either enhanced or reduced due to electrostatics depending on the charge on the nanoparticles as compared to the purely diffusional case of an uncharged particle.

4.2 Electrode Potential

This section revisits the experimental scenario discussed in the previous section. However, rather than the nanoparticle charge, we vary the electrode potential and determine its effect on the rate of reacting particles j_e . Figure 4 presents the numerical solution to j_e for particles that carry a charge of 50 and feature a radius of 100 nm. The Debye length is again set to 100 nm, which corresponds to 9.42 μM of a

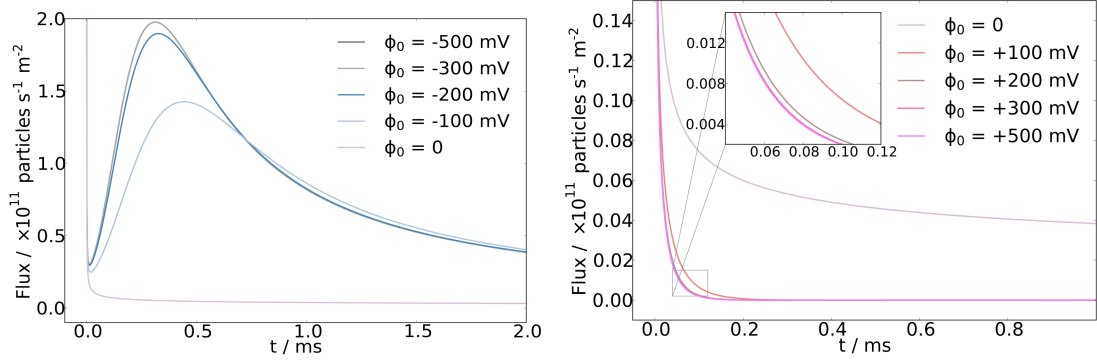


Figure 4: a) Comparison of the flux at different negative electrode potentials. The graphs corresponding to -500 mV and -300 mV overlap. b) Comparison of the flux for different positive electrode potentials. The curves corresponding to 500 mV and 300 mV overlap. In all simulations, the nanoparticle charge is 50, the Debye length is 100 nm, which corresponds to $9.42 \mu\text{M}$ of a 1:1 monovalent supporting electrolyte, and the particle radius is 100 nm.

1:1 monovalent supporting electrolyte.

As shown in Figure 4 a) and b), the rate of reaction j_e decreases as the electrode potential increases. In addition, we observe a peak when the applied potential is equal to or smaller than -100 mV. The decrease in j_e is due to the increasing electrostatic repulsion of the positively charged particles from the increasingly positive electrode, which reduces the mass transport towards it. The explanation of the peak follows Section 4.1 where we have established that the peak arises from the combination of the enhanced nanoparticle migration from the bulk solution and the retarded mass transport near the interface due to hindered diffusion which leads to a temporal up concentration of nanoparticles in the vicinity of the electrode that reflects in the peak.

Another notable feature of Figure 4 is the observation that when the electrode potential is more negative than -300 mV or greater than 300 mV, the change in the electrode potential does not result in significant changes of the particles rate of reaction. Figure 5 further illustrates that when the electrode potential is lowered from -300 mV to -500 mV, the concentration profiles of nanoparticles remain unchanged. To explain this finding, we consider how the potential ϕ varies in solution and exemplarily plot the potential in solution for various negative electrode potentials ϕ_0 in Figure 6.

The figure reveals that when ϕ_0 is more negative than -300 mV, not only the variation of the particle concentration but also the potential remain unchanged. While this might possibly be counter-intuitive, the unchanged potential can be easily understood by the mathematical structure of ϕ in the Gouy-Chapman model (11): ϕ is a function of $\tanh(\theta_0/4)$, where θ_0 is the dimensionless potential applied at the electrode. If $|\theta_0|$ adopts large values, the corresponding values of $|\tanh(\frac{\theta_0}{4})|$ for different θ_0 converge to unity and above a certain threshold equal each other within the numerical precision of the 64-bit

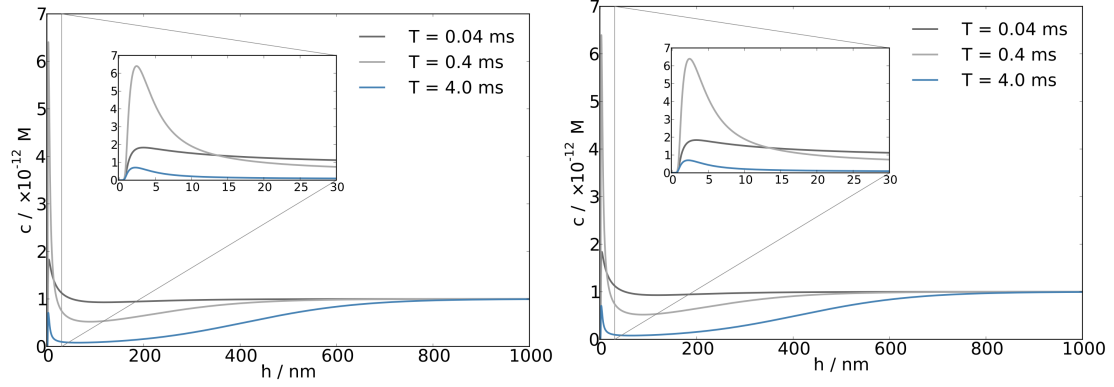


Figure 5: Concentration profiles at different times calculated for electrode potentials of a) -300 mV and b) -500 mV. All other parameters used equal the parameters set in Figure 4.

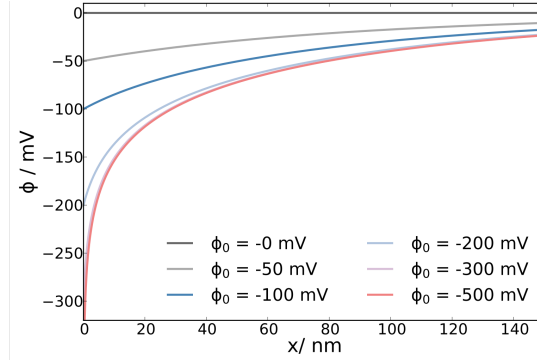


Figure 6: The variation of solution potential with the distance from the electrode evaluated for different negative electrode potentials ϕ_0 . Note that the graphs corresponding to $\phi_0 = -300 \text{ mV}$ and $\phi_0 = -500 \text{ mV}$ overlap.

variables used in our numerical model. Hence, spatial potential distributions are identical and identical reaction rates are observed.

In summary, this section has been demonstrated that if applied over- or under-potentials exceed a threshold value of around $\pm 300 \text{ mV}$, further increases in the magnitude of the electrode potential do not significantly change the mass transport of nanoparticles towards the electrode.

4.3 Nanoparticle Radius

In the following, we investigate the effect of the nanoparticle radius. Reaction rates evaluated for different nanoparticle radii (1 - 100 nm) are presented in Figure 7. A case constructed for no hindered diffusion, where the particle radius is set to be 1 \AA and the diffusion coefficient is simply calculated via the Stokes-Einstein equation (9), is additionally included in the figure. We though note that in this scenario, the assumption of a potential gradient being instantaneously established relative to the time scale of the

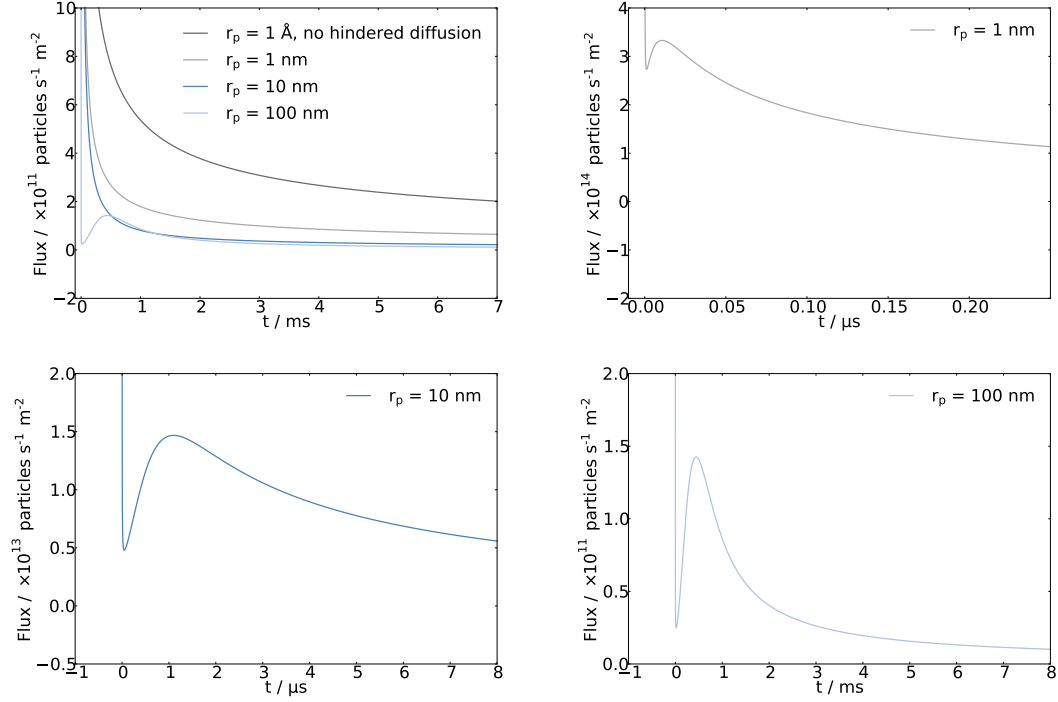


Figure 7: Flux simulated for different nanoparticle radii, r_p . a) Comparison of different radii and the case of no hindered diffusion. b), c) and d) Amplified plots of the data shown in a). Nanoparticles carry the charge 50, the electrode potential is -100 mV and the Debye length is 100 nm, which corresponds to $9.42 \text{ } \mu\text{M}$ of a 1:1 monovalent supporting electrolyte. Note that the amplified graphs are plotted for different time scales and different magnitudes of flux to highlight aspects of interest.

particle mass transport is invalid. The case is nonetheless of interest as this diffusion model still remains common in the literature. Nanoparticles carry the charge 50, the electrode potential is -100 mV and the Debye length is 100 nm, which corresponds to $9.42 \text{ } \mu\text{M}$ of a 1:1 monovalent supporting electrolyte.

As can be seen from Figure 7 a), the reaction rate decreases as the particle radius increases, with the rate of the non-hindered case being the greatest. This can be understood as for the cases of hindered diffusion, the diffusion coefficient drops near the electrode surface and hence the mass transport slows down. Moreover, following the Stokes-Einstein equation (9), the bulk diffusion coefficient, D_∞ , decreases with increasing particle radii. Since $D(x)$ is proportional to D_∞ , the mass transport of larger particles in terms of both diffusion and migration becomes slower, and the reaction rate decreases.

In the Figures 7 b), c) and d), peaks are seen in the calculated reaction rates. The explanation of the peaks, again, follows Section 4.1, and is understood as the result of enhanced nanoparticle migration from the bulk solution and the retardation of mass transport near the interface due to hindered diffusion. As the nanoparticle size increases, these peaks appear at later times and their duration increases. To further investigate this observation, we look into the concentration profiles at different times.

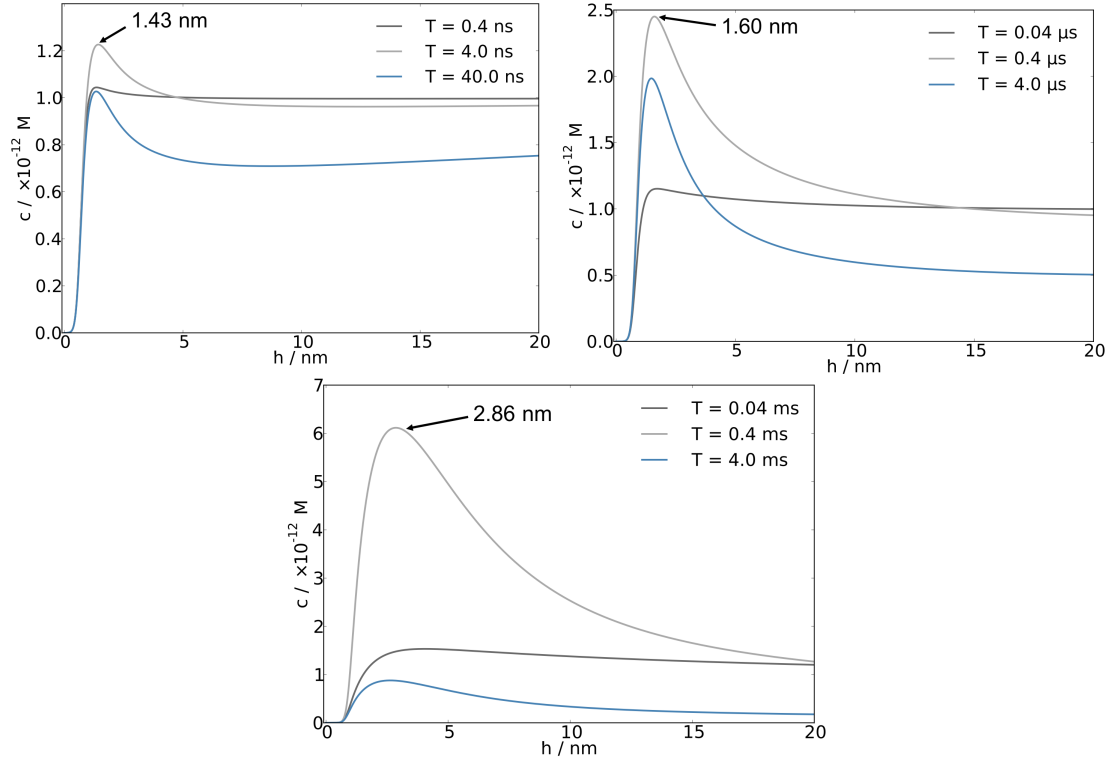


Figure 8: Concentration profiles for different nanoparticle radii, r_p . Concentration profiles when the nanoparticle radius is a) 1 nm, b) 10 nm, and c) 100 nm. Numbers drawn in the figures indicate exact peak positions. All other parameters equal the parameters used in Figure 7.

Figure 8 shows the concentration profiles evaluated at different time for nanoparticles featuring different radii. Contrary to possible expectations, the up-concentrations occur at later times and the extent of up-concentration with respect to the bulk concentration increases as the nanoparticles becomes larger. The up-concentration can thus be controlled simply by altering the radius of the nanoparticles used. In this context, the varied appearance of the peaks in the reaction rate can be explained by variations of the extent of accumulation with time. As the nanoparticle size increases, the diffusion coefficient decreases according to the Stokes-Einstein relation (9), which reduces the rates of diffusion and migration. The mass transport of nanoparticles with larger radii is therefore slower, which results in a slower building of the concentration and thus the later appearance of peaks in the reaction rate. Moreover, larger nanoparticles are prone to more pronounced hindered diffusion (see Equation (8)), which results in a slower mass transport to the electrode surface and thus the slower removal of nanoparticles from the accumulation region. The duration of the peaks is hence longer as the particle size increases.

Figure 8 further shows that the position of the concentration peak moves away from the electrode as the nanoparticle radius increases. As particles become larger, the effect of hindered diffusion becomes more pronounced and the diffusion coefficient begins to decrease significantly from positions further away

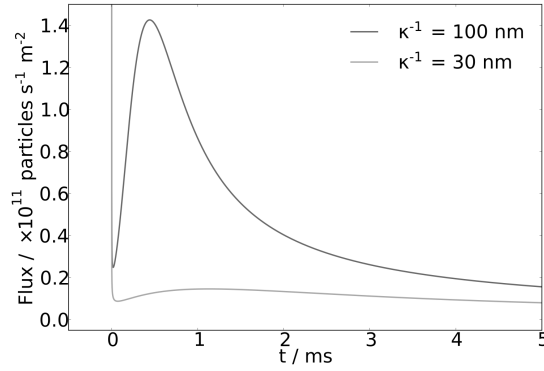


Figure 9: Comparison of the reaction rate when the Debye length is 100 nm and 30 nm, which corresponds to 105 μM and 9.42 μM of a 1:1 monovalent supporting electrolyte. The nanoparticle charge is 50, the electrode potential is -100 mV and the particle radius is 100 nm.

from the electrode. The region in which particles accumulate is therefore located further away from the electrode.

To summarise, this section has established the relation between the nanoparticle radius and the appearance of peaks in the flux: the larger the nanoparticle is, the later the peak is observed and the longer it lasts.

4.4 Debye Length

Last but certainly not least, the effect of the Debye length on the flux is investigated. The Debye length can be controlled simply by altering the amount of electrolytes added in the solution and is hence easily controlled in experiments. The potential drop confined to the proximity to the interface is characterised by the Debye length, which is given by Equation 12, and features an inverse proportionality to the square root of the electrolyte concentration. Here, the flux is simulated for two different Debye lengths: 30 nm and 100 nm, which correspond to 105 μM and 9.42 μM of 1:1 monovalent supporting electrolyte respectively. The nanoparticles are assumed to carry a charge of 50, the electrode potential is -100 mV and the particle radius is 100 nm.

Figure 9 illustrates the simulated fluxes and a peak in flux is observed in both cases. It is further revealed that as the Debye length increases, the flux increases within the investigated time interval. This can be understood via an analysis of the electric field, $\nabla\phi$, in the solution at different Debye lengths.

As illustrated in Figure 10, as the Debye length increases, the potential drop occurs over a larger distance and thus the electric field penetrates further into the solution while the magnitude of the electric field near the interface decreases. The increase in the penetration depth of the electric field however outweighs the latter effect and the mass transport of nanoparticles due to migration is enhanced as the

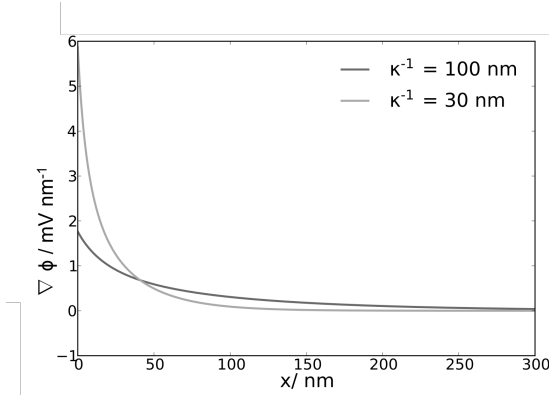


Figure 10: Variation of absolute electric field strength, $|\nabla\phi|$, with distance from the electrode surface at different Debye lengths.

Debye length increases. The formation of the flux peak, as explained in Section 4.1, is again the result of the elevated migration of nanoparticles from the bulk solution to the electrode due to the electric field present in the solution in combination with the hindered diffusion near the electrode.

In summary, this section has revealed that by changing the Debye length from 30 nm to 100 nm, which corresponds to a ten-fold decrease in the 1:1 monovalent supporting electrolyte concentration, an increase in the amplitude of the flux by more than 14 times is observed. The mass transport and the up-concentration of nanoparticles can hence be dramatically enhanced by simply reducing the concentration of background electrolytes.

5 Conclusions

This work, for the first time, investigates the combined effect of electrostatics *and* hindered diffusion in a particle electrochemistry context. A new theoretical model based on the Nernst-Planck equation, the Gouy-Chapman model, and a well-validated model for near-wall hindered diffusion is developed and numerically solved to understand the mass transport.

Entirely new physical insights into the mass transport of nanoparticles have been achieved: Most notably, an accumulation of nanoparticles at a well-defined distance from the electrode surface is predicted and attributed to the interplay between near-wall hindered diffusion and electrostatics: Nanoparticles approach the electrode by virtue of migration while the mass transport further on to the electrode is retarded by hindered diffusion. We additionally demonstrate that the mass transport of charged nanoparticles to the electrode can be accelerated by the choice of an appropriate electrode potential while small over- or under-potentials are sufficient and potentials beyond a threshold of about ± 300 mV

do not further improve the mass transport.

Conflicts of Interest

There are no conflicts of interest to declare.

Acknowledgements

The research leading to these results has received partial funding from the European Research Council under the European Union’s Seventh Framework Programme (FP/20072013) / ERC Grant Agreement no. [320403].

References

- [1] S. V. Sokolov, S. Eloul, E. Kätelhön, C. Batchelor-McAuley and R. G. Compton, *Physical Chemistry Chemical Physics*, 2017, **19**, 28–43.
- [2] M. V. Mirkin, T. Sun, Y. Yu and M. Zhou, *Accounts of Chemical Research*, 2016, **49**, 2328–2335.
- [3] P. H. Robbs and N. V. Rees, *Physical Chemistry Chemical Physics*, 2016, **18**, 24812–24819.
- [4] C. Batchelor-McAuley, E. Kätelhön, E. O. Barnes, R. G. Compton, E. Laborda and A. Molina, *ChemistryOpen*, 2015, **4**, 224–260.
- [5] W. Cheng and R. G. Compton, *TrAC Trends in Analytical Chemistry*, 2014, **58**, 79–89.
- [6] Y.-G. Zhou, N. V. Rees, J. Pillay, R. Tshikhudo, S. Vilakazi and R. G. Compton, *Chem. Commun.*, 2012, **48**, 224–226.
- [7] L. Sepunaru, B. J. Plowman, S. V. Sokolov, N. P. Young and R. G. Compton, *Chemical Science*, 2016, **7**, 3892–3899.
- [8] L. Sepunaru, K. Tschulik, C. Batchelor-McAuley, R. Gavish and R. G. Compton, *Biomaterials Science*, 2015, **3**, 816–820.
- [9] E. Kätelhön, L. Sepunaru, A. A. Karyakin and R. G. Compton, *ACS Catalysis*, 2016, **6**, 8313–8320.
- [10] C. Lin, E. Kätelhön, L. Sepunaru and R. G. Compton, *Chemical Science*, 2017, **8**, 6423–6432.

- [11] S. Lior, S. S. V., H. Jennifer, Y. N. P. and C. R. G., *Angewandte Chemie International Edition*, 2016, **55**, 9768–9771.
- [12] M. Park, J. Ryu, W. Wang and J. Cho, *Nature Reviews Materials*, 2017, **2**, 16080.
- [13] G. L. Soloveichik, *Chemical Reviews*, 2015, **115**, 11533–11558.
- [14] M. Duduta, B. Ho, V. C. Wood, P. Limthongkul, V. E. Brunini, W. C. Carter and Y.-M. Chiang, *Advanced Energy Materials*, 2011, **1**, 511–516.
- [15] V. Presser, C. R. Dennison, J. Campos, K. W. Knehr, E. C. Kumbur and Y. Gogotsi, *Advanced Energy Materials*, 2012, **2**, 895–902.
- [16] E. O. Barnes and R. G. Compton, *Journal of Electroanalytical Chemistry*, 2013, **693**, 73–78.
- [17] S. Eloul and R. G. Compton, *The Journal of Physical Chemistry Letters*, 2016, **7**, 4317–4321.
- [18] S. Eloul, E. Kätelhön and R. G. Compton, *Physical Chemistry Chemical Physics*, 2016, **18**, 26539–26549.
- [19] K. B. Oldham and C. G. Zoski, *Electrode Kinetics: Principles and Methodology*, Elsevier, 1986, vol. 26, pp. 79 – 143.
- [20] M. B. Rooney, D. C. Coomber and A. M. Bond, *Analytical Chemistry*, 2000, **72**, 3486–3491.
- [21] M. Ciszowska and Z. Stojek, *Journal of Electroanalytical Chemistry*, 1999, **466**, 129 – 143.
- [22] E. J. F. Dickinson, J. G. Limon-Petersen, N. V. Rees and R. G. Compton, *Journal of Physical Chemistry C*, 2009, **113**, 11157–11171.
- [23] J. G. Limon-Petersen, J. T. Han, N. V. Rees, E. J. F. Dickinson, I. Streeter and R. G. Compton, *Journal of Physical Chemistry C*, 2010, **114**, 2227–2236.
- [24] S. Eloul, E. Kätelhön, C. Batchelor-McAuley, K. Tschulik and R. G. Compton, *Journal of Physical Chemistry C*, 2015, **119**, 14400–14410.
- [25] R. G. Compton, E. Laborda and K. R. Ward, *Understanding Voltammetry: Simulation of electrode processes*, Imperial College Press, 2013.
- [26] M. A. Bevan and D. C. Prieve, *The Journal of Chemical Physics*, 2000, **113**, 1228–1236.
- [27] M. V. Fedorov and A. A. Kornyshev, *Chemical Reviews*, 2014, **114**, 2978–3036.

- [28] E. Kätelhön, E. E. Tanner, C. Batchelor-McAuley and R. G. Compton, *Electrochimica Acta*, 2016, **199**, 297–304.
- [29] S. Eloul, E. Kätelhön and R. G. Compton, *Physical Chemistry Chemical Physics*, 2016, **18**, 26539–26549.
- [30] S. V. Sokolov, E. Kätelhön and R. G. Compton, *The Journal of Physical Chemistry C*, 2016, **120**, 10629–10640.
- [31] P. P. Edwards, H. B. Gray, M. T. J. Lodge and R. J. P. Williams, *Angewandte Chemie International Edition*, 2008, **47**, 6758–6765.